Astron. Astrophys. 334, 1060–1067 (1998)

ASTRONOMY AND ASTROPHYSICS

Study of the Rayleigh-Taylor instability in Tycho's supernova remnant

P.F. Velázquez[1,⋆], **D.O. Gómez**[1,2], **G.M. Dubner**[1], **G. Giménez de Castro**[1,⋆⋆,⋆⋆⋆], **and A. Costa**[1,†]

[1] Instituto de Astronomía y Física del Espacio, CC 67, Suc. 28, 1428 - Buenos Aires, Argentina
(pablov@iafe.uba.ar, gomez@iafe.uba.ar, gdubner@iafe.uba.ar, costa@iafe.uba.ar)
[2] Department of Physics, University of Buenos Aires, Argentina

Received 13 January 1998 / Accepted 4 March 1998

Abstract. In the present paper we investigate the linear stage of instabilities which might take place at the shock front of young supernova remnants (hereafter SNR), deriving expressions for the characteristic wavelength and typical growth time scales. These theoretical predictions are compared with very high resolution observations of Tycho's SNR obtained with the Very Large Array at 1.4 GHz. The images obtained with an angular resolution of the order of 1 arcsec and with very good sensitivity, clearly reveal the presence of corrugated (wavelike) structures with remarkable spatial regularity, visible mainly along the northeastern part of the SNR shell. We argue that the Rayleigh-Taylor instability (hereafter R-T) is responsible for the observed structures. Using physical parameters of Tycho's remnant and its environment derived from different X-ray observational studies, we computed the expected wavelength and growth rate for the most unstable R-T mode including viscosity and magnetic effects. The wavelength we derive is fully compatible with the one measured directly on the image ($\lambda_{obs} \sim 0.9\,\mathrm{pc}$). The growth rate derived for this mode indicates that the R-T instability is still undergoing its linear stage.

Key words: ISM: supernova remnants – shock waves – ISM: individual: Tycho SNR – hydrodynamics – instabilities

1. Introduction

A supernova explosion can be described as the sudden release of a very hot gas into the interstellar medium (hereafter ISM). As it evolves, it can be seen as a non-thermal source in radio wavelengths (synchrotron radiation) and sometimes emitting in the optical, infrared and X-ray ranges. The residues left after the explosion, which can be traced through the emission processes listed above, are known as a supernova remnant (SNR). For hundreds of years, the ejected material expands into the surrounding medium, colliding with the circumstellar environment. Later, as the remnant continues to expand, it interacts with the local ISM and, as a result, a combination of SN ejecta with processed ISM is observed.

The encounter between the shock front created by the supersonic blast wave, and the circumstellar environment leads to a multilayer structure, with two shock fronts. Namely, from inside to outside: an inner or reverse shock where the ejected material decelerates, a region of hot ejectum that has passed through the reverse shock, a contact surface, a region of shocked ISM, and finally, an outer or main shock. Once the interstellar material pushed by the contact discontinuity (and accumulated ahead of it) is massive enough, it becomes a source of deceleration for the ejected material, thus setting the conditions for the R-T instability to grow. The study of the radio morphology of SNRs in the early stages of evolution should in principle help to identify unstable regions, since the synchrotron emission is enhanced where the magnetic field lines become more compressed and the relativistic particles are accelerated.

In the present work we analyze the feasibility of the development of the R-T instability, in the remnant of the Tycho SNR (also known as 3C10). The observational part of the study is based on very high resolution and sensitivity observations of 3C10 conducted by Reynoso et al. 1997 at 1.4 GHz using the Very Large Array (VLA) [1] as part of an extensive study of the expansion of this remnant. In particular, the image obtained in the A-array, with an angular resolution of $1''.4$, shows with unprecedented detail the presence of very regularly distributed features with a wavelike morphology, right behind the outer rim. Such a spatial structure, more clearly revealed along the north-eastern border of the remnant (see Fig. 1), suggests that this young SNR is undergoing the initial stages of an instability.

In the present work we explore the feasibility of R-T instability for the shocked gas in Tycho's remnant. For reasonable values of its physical parameters we obtain: (a) that the con-

Send offprint requests to: P.F. Velázquez
⋆ Fellow of CONICET
⋆⋆ Fellow of CNPq, Brasil
⋆⋆⋆ *Present address:* NUCATE, Universidade Estadual de Campinas, Rua Roxo Moreira 1752, 13083 - 592, Campinas, SP, Brasil (guigue@nucate.unicamp.br)
† Gómez, Dubner and Costa are Members of the Carrera del Investigador Científico, CONICET, Argentina

[1] The Very Large Array of the National Radio Astronomy Observatory is a facility of the N.S.F. operated under cooperative agreement by the Associated Universities Inc.

ditions for R-T instability are indeed satisfied by the contact discontinuity and, (b) the wavelength and rise time of the most unstable mode are consistent with the spacing of the wavelike structure observed and the presumed lifetime for this unstable condition.

Recent images of the Crab Nebula obtained with the Hubble Space Telescope (Hester et al. 1996), show a variety of optical filaments, which were tentatively associated to fingers corresponding to a largely nonlinear stage of a R-T instability. In the case of Tycho's SNR, the radio wavelike features have a considerably smaller amplitude, supporting our assumption that the instability is still in the early stages of its development.

The work is organized as follows. In Sect. 2 we briefly describe the observational database. In Sect. 3 we summarize the theoretical background, reviewing the piston model for SNRs and the R-T instability, considering the viscous and magnetic effects on its development. In Sect. 4 we show the results obtained for the particular case of Tycho's SNR, and in Sect. 5 we list our conclusions.

2. The observations

The radio observations discussed in the present work were performed with the VLA in all four spatial configurations at 1375 and 1635 MHz for 55 hours along 1994 and 1995 by Reynoso et al. 1997. The synthesized beam turned out to be $1.4''$, which is equivalent to 0.03 pc at an adopted distance to Tycho's SNR of 4.6 kpc (Schwarz et al. 1995). The rms noise is about 110 μJy/beam.

Fig. 1 shows the VLA image of Tycho's SNR as taken from Reynoso et al. 1997. The remnant is highly symmetric in most of its periphery, only departing form a spherical shape toward the North and East. Precisely along the NE, the presence of a wavy structure can be noticed. This structure, formed by small and very regularly spaced "protrusions", is located behind the outer shock front.

In Fig. 2 we display an enlargement of this area with a greyscale adequate to emphasize fainter features. The equally spaced set of arrows point to the crest of the waves. The spacing is denoted by λ. Although projection effects can slightly alter the morphology, the uniformity of these structures is remarkable. We interpret these small features, which appear to be growing outwards, as the heads of incipient R-T fingers. The only irregularities in the pattern can be seen in the second crest from north to east (see Fig. 2), whose growth seems to be delayed with respect to the others, and the presence of an extension or "plume" in front of the sixth crest, whose origin is not clear.

Note that the presence of such fingers toward the NE of Tycho's SNR is consistent with Reynoso et al.'s 1997 results who, based on a study of the expansion of this remnant on a ten years interval, conclude that the NE region is currently the slowest section of the whole source. This fact, together with the position and shape of optical filaments, are interpreted as evidences of a local higher upstream density. A study of the surrounding neutral gas performed by Reynoso et al. 1998 reveals in fact the existence of a denser HI cloud slowing down the propagation of the shock front towards the NE. Therefore, if the shock front encountered a region somewhat denser than average, this will naturally be the first place to search for signs of R-T instability. Also, an inhomogeneous distribution of the different chemical species along the rim, as reported by Hwang & Gotthelf 1997, might affect the evolution of R-T instability.

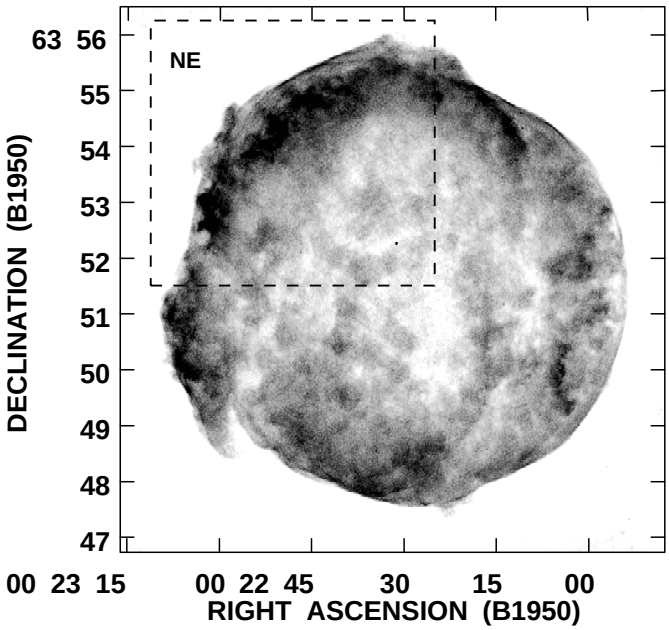

Fig. 1. Image of the Tycho remnant, at 1.4 GHz as obtained with the A, B, C and D configurations of the VLA (Reynoso et al. 1997). The inner frame indicates the region shown in Fig. 2

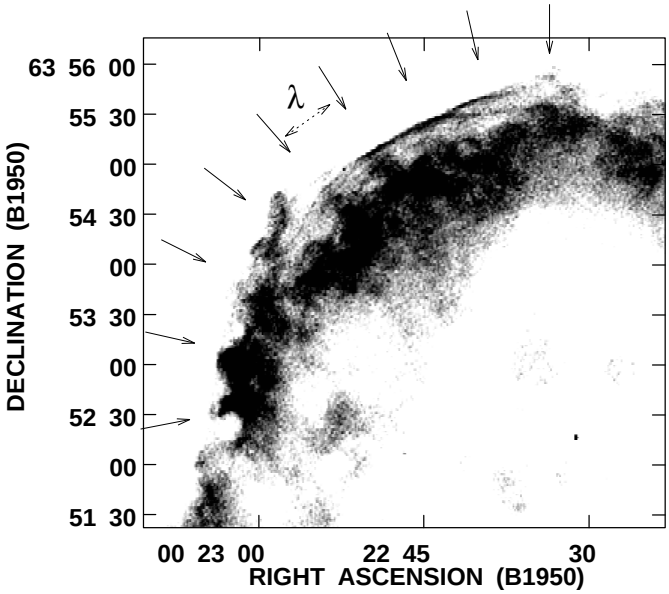

Fig. 2. Image of northeastern quadrant of Tycho's SNR, at 1.4 GHz, as taken with the VLA in the A, B, C and D configurations.

3. Theoretical background and comparison with observations

3.1. The Piston model

The physical configuration of SNRs changes several times throughout their evolution. These changes can be described in terms of evolutionary stages. Woltjer 1970 (also Raymond 1984) characterizes the expansion of a SNR in four stages: (i) the **free expansion** stage of the gas, during which the radius R for the contact discontinuity expands like $R \propto t$; (ii) the **piston** stage in which the swept-up mass is larger than the ejected mass, described by the similarity solution of Taylor 1950 and Sedov 1959 ($R \propto t^{2/5}$); (iii) the **snowplough** stage given by an expansion law $R \propto t^{1/4}$ and (iv) the **dispersion** stage, where the velocity becomes smaller than the sound speed, the expansion slows down and the remnant loses its shell-like structure. During the **piston** stage, the temperature of the gas behind the shock becomes so high that radiative losses can be neglected, since the hydrodynamic time is shorter than the cooling time. Therefore, during this phase of its evolution, the SNR expands adiabatically. On the other hand, the main characteristic of the **snowplough** stage, is that radiative cooling is dominant, causing the temperature to fall quite rapidly and inducing the shock to become isothermal. This process originates the formation of a dense shell right behind the shock front.

The first two stages of the expansion were extensively studied by Gull 1973. He has shown that for any reasonable specification of the initial explosion in which the energy is suddenly released, a contact discontinuity must form at the boundary between the ejecta and the interstellar material. Contact discontinuities are characterized by a zero flow across them. Therefore, the material ejected by the star plays the role of a **piston** (indicated by R_p in Fig. 3), pushing the interstellar material ahead as it evolves. Connected with this behavior, there is a **blast wave** propagating ahead of the piston, indicated by R_s in Fig. 3. Also, there is a **reverse shock**, propagating backward in the medium formed by the ejected material.

The natural candidate for the growth of the R-T instability is the contact discontinuity between the piston (the ejected material) and the shocked ISM, as shown in Fig. 3. The adiabatic blast shock, marked as R_s, is stable for typical values of the polytropic index $\Gamma = c_p/c_v$, as pointed out by Newman 1980 (also Landau & Lifshitz 1959).

3.2. The Rayleigh-Taylor instability

The R-T instability occurs when heavy fluid lies over a lighter one, in the presence of a gravitational field. Via the Equivalence Principle, the R-T instability also takes place whenever a heavy fluid is accelerated by a lighter fluid. The R-T instability develops in a variety of astrophysical contexts, including supernova explosions (Fryxell et al. 1991), the interaction of shock waves with dense clouds present in the ISM (Stone & Norman 1992), and in the shells of young SNRs (Chevalier et al. 1992, Jun et al. 1995). This problem has been studied analytically (Chandrasekhar 1961, Friedman 1954), experimentally (Read 1984), and numerically (Gardner et al. 1988, Glimm et al. 1990, Li 1993, Sharp 1984, Youngs 1984). A good summary of these studies and of the astrophysical contexts where the R-T instability manifests itself, can be found in Jun et al. 1995.

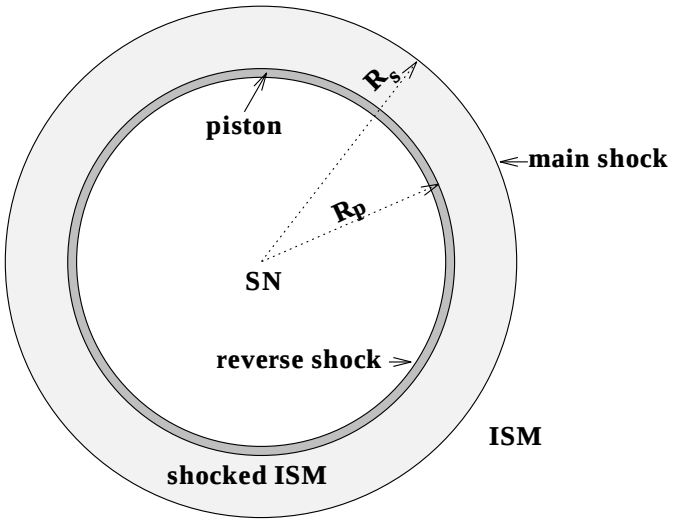

Fig. 3. Sketch of the structure of a SNR.

A stability analysis of spherically symmetric self-similar equilibria was presented by Chevalier et al. 1992, to describe the dynamics of young SNR shock fronts propagating in uniform ISM. They perform a decomposition in terms of spherical harmonics and show the development of unstable flows for values of *l* above a critical threshold. However, since they do not include viscosity in their model, the spectrum of unstable modes is broadband.

In this paper we consider a very simple model, which can easily be compared with high quality observations from different SNRs. It consists of two incompressible, inviscid and unmagnetized fluids of densities ρ_1 and ρ_2, separated by a contact discontinuity perpendicular to the effective gravitational field $\mathbf{g}$, where ρ_1 and ρ_2 are the densities of the light and heavy fluids, respectively.

The growth rate of the R-T instability is given by:

$$\gamma(k) = \sqrt{k\, g\, (\alpha_2 - \alpha_1)} \tag{1}$$

where k is the wavenumber of the perturbation, $\alpha_{1,2} = \rho_{1,2}/(\rho_2 + \rho_1)$, and g represents the effective gravitational intensity. From this equation, we note that the growth rate $\gamma(k)$ diverges for $k \to \infty$ ($\lambda \to 0$). Various physical factors which can influence the development of this instability, have been ignored in the derivation of Eq. (1), such as fluid viscosity, compressibility and magnetic fields, all of which play a stabilizing role. Fluid viscosity is a dissipative mechanism that produces preferential damping at small wavelengths (Plesset & Whipple 1974). Compressibility also inhibits the development of the instability, but its contribution becomes negligible for small wavelength perturbations (Blake 1972). The effects of a magnetic field in the linear regime have been studied analytically by Chandrasekhar 1961.

If the magnetic field is parallel to the interface, its role is analogous to a surface tension, which therefore contributes to stabilize the fluid. When the magnetic field is predominantly normal to the interface, it tends to stabilize the fluid, specially at large wavenumbers. The situation becomes more complex when nonlinear effects need to be taken into account. Normal magnetic fields in this case tend to increase the growth rate of the R-T fingers (Jun et al. 1995), which are nonlinear structures generated as a result of the intrusion of one fluid into the other. Observational evidence of the presence of these nonlinear structures has recently been reported by Hester et al. 1996 in the Crab Nebula, based on *Hubble Space Telescope* WFPC2 optical images, in the form of long R-T fingers pointing inwards. Such R-T fingers have originated through the interaction between the pulsar-driven synchrotron nebula and the ejecta from the explosion. It is important to note that although both Tycho's SNR and the Crab Nebula are proposed to undergo a R-T instability, the physical conditions are quite different, mainly because the Crab SNR is much older than Tycho's SNR and has a central pulsar. Therefore, the different scenarios can explain the various morphological differences between the two cases.

In the following subsections we briefly discuss the roles of viscosity and magnetic fields in the development of the R-T instability, which might be non-negligible for young SNRs like Tycho.

3.3. Effect of fluid viscosity

Viscosity should not be ignored at small wavelengths. Note from Eq. (1) that the growth rate $\gamma(k)$ displays a spurious divergent behavior for $k \to \infty$ ($\lambda \to 0$). Viscous corrections to the growth-rate can be taken into account in our calculations following simple physical arguments (Plesset & Whipple 1974 and Cowie 1975). The growth rate is given by the positive root of:

$$\gamma^2 + 2\nu k^2 \gamma - k\, g\, (\alpha_2 - \alpha_1) = 0 \tag{2}$$

where ν is the kinematic viscosity.

From Eq. (2) it is apparent that viscosity damps stable and unstable interfacial waves, since it resembles the familiar expression for a damped harmonic oscillator.

We readily find that $\gamma(k)$ has a maximum at

$$k_* = \frac{2\pi}{\lambda_*} = \frac{1}{2}\left(\frac{g}{\nu^2}(\alpha_2 - \alpha_1)\right)^{1/3} \tag{3}$$

and

$$\gamma_* = \frac{1}{\tau_*} = \frac{1}{2}\left(\frac{g^2}{\nu}(\alpha_2 - \alpha_1)^2\right)^{1/3} \tag{4}$$

where γ_* is the maximum value for γ.

Note that the existence of this maximum is determined by the viscosity of the fluid, which in turn is a strong function of the temperature. In Sect. 4 we associate the characteristics of this fastest growing mode, to the wavelike structures observed at the NE shock front of Tycho's remnant.

As mentioned before, for the particular case of SNRs, the piston material is continuously being decelerated by the compressed and shocked gas and therefore the contact surface in between becomes a candidate for the R-T instability. Via the Equivalence Principle, this deceleration will be sensed by the fluid at the interface as an effective gravitational field.

As long as the piston density remains larger than the density of the shocked ISM, the R-T instability will grow at a rate derived from Eq. (2).

For high temperature and low density plasmas, the viscosity coefficient is (Spitzer 1962):

$$\nu = 3.5 \times 10^7 \frac{T_p^{5/2}}{4\, n_p}\ \mathrm{cm^2\ s^{-1}} \tag{5}$$

where T_p and n_p are respectively the piston temperature and density.

The observational implications of Eqs. (3) and (4) are the following: the interfacial disturbance with the particular wavelength $\lambda_* = 2\pi/k_*$ will grow faster than any other. Its growth will become noticeable in a typical timescale $\tau_* = 1/\gamma_*$.

Let us write down these quantities in terms of parameters which can be inferred from observations. We define the following dimensionless quantities:

$$T_7 = \frac{T_p}{10^7\ K}, \tag{6}$$

$$n_1 = \frac{n_p}{1\ cm^{-3}}, \tag{7}$$

$$g_2 = \frac{g_{eff}}{10^{-2}\ cm.s^{-2}}, \tag{8}$$

$$\alpha = \frac{\rho_p - \rho_s}{\rho_p + \rho_s} = \frac{n_p - n_s}{n_p + n_s} \tag{9}$$

where ρ_s and ρ_p represent the densities ahead and behind the interface. In terms of these dimensionless quantities, we obtain

$$\lambda_* = 0.39\left(\frac{T_7^5}{g_2\ \alpha\ n_1^2}\right)^{1/3}\ \mathrm{pc}, \tag{10}$$

$$\tau_* = 190\left(\frac{T_7^{5/2}}{n_1\ \alpha^2\ g_2^2}\right)^{1/3}\ \mathrm{years} \tag{11}$$

We compare the growth rate of the R-T instability with and without viscosity in Fig. 4. The viscous case is considered for different temperatures. In Fig. 4 we can observe that larger temperatures tend to stabilize the fluid, and shift λ_* shigthly to larger values.

3.4. Magnetic field effects

The presence of magnetic fields has two effects on the evolution of the R-T instability: (1) the fluid equations to be satisfied in the neighborhood of the contact discontinuity must include magnetic forces, and an induction equation should be added to describe the dynamics of the magnetic field itself, (2) the microscopic transport of momentum becomes anisotropic, which

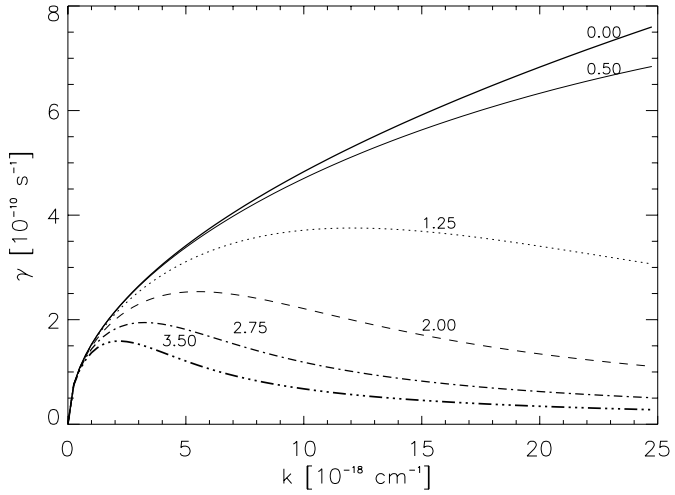

Fig. 4. R-T instability including viscosity with g_2=7.0, $d_1 = 1.9$, α=0.33. The labels correspond to different values for the temperature T_7.The thick trace correspond to the viscous-free case.

requires to replace the viscosity coefficient by a tensor quantity. The implications of these two effects are briefly discussed in subsections Sect. 3.4.1 and Sect. 3.4.2, respectively.

3.4.1. Effect on the dynamics of the interface

The role of a uniform magnetic field **H** forming an angle β with the normal to the contact discontinuity surface, has been studied by Chandrasekhar 1961. To this end, the fluid equations need to be extended to the magnetohydrodynamic (MHD) equations, which consistently describe the dynamics of both the velocity and magnetic fields.

Using the ideal MHD equations (i.e. without dissipation, the role of viscosity will be discussed in the next subsection) to compute the matching conditions at the contact discontinuity, yields the following equation for the instability rate

$$\gamma^3 + c_2\,\gamma^2 + c_1\,\gamma + c_0 = 0 \tag{12}$$

where

$$c_2 = 2\,k\,V_A\,cos\beta\,\chi\,(\sqrt{\alpha_1}+\sqrt{\alpha_2}) - 4\,i\,tan\beta\,V_A\,cos\beta\,k\,\frac{\sqrt{\alpha_1\alpha_2}}{\sqrt{\alpha_1}+\sqrt{\alpha_2}} \tag{13}$$

$$c_1 = 2(k\,V_A\,cos\beta\,\chi)^2 - 4\,i\,tan\beta\,\chi\,(V_A\,cos\beta\,k)^2 - k\,g\,(\alpha_2-\alpha_1) \tag{14}$$

$$c_0 = 2\,k^2\,V_A\,cos\beta\,\chi\,(\sqrt{\alpha_2}-\sqrt{\alpha_1}) - 4\,i\,\frac{tan\beta\,\chi^2\,(k\,V_A\,cos\beta)^3}{\sqrt{\alpha_1}+\sqrt{\alpha_2}} \tag{15}$$

The constant V_A in Eqs. (12-15) is the Alfven velocity ($V_A = H/\sqrt{4\,\pi\,(\rho_2+\rho_1)}$), and $\chi = 1 - i\,tan\beta$. Note that for $H \to 0$, Eq. (12) reduces to Eq. (1)

3.4.2. Anisotropization of viscosity

Viscous forces are the macroscopic manifestation of the microscopic transport of momentum carried by particles and driven by gradients in the fluid velocity field. In the absence of a magnetic field, the intensity of this transport is fully described by the viscosity coefficient given in Eq. (5). The presence of a magnetic fields breaks the isotropy of momentum transport, and therefore the role of viscosity is represented by a viscous tensor. Physically, the anisotropy is caused by the spiral motion of charged particles along magnetic field lines. Although the transport along field lines remains unaffected, the transport across field lines can be seriously reduced for intense magnetic fields. More specifically, the viscous tensor has five independent coefficients:

$$\nu_0 = \nu\ ;\ \nu_1 \sim \nu_2 \sim \frac{\nu}{(\omega_c\tau)^2}\ ;\ \nu_3 \sim \nu_4 \sim \frac{\nu}{\omega_c\tau} \tag{16}$$

(see Braginskii 1966). Note that the limitation in transverse transport is determined by the dimensionless factor $\omega_c\,\tau$, where $\omega_c = \frac{e\,H}{m\,c}$ is the ion cyclotron frequency (e is the electron charge and m is the ion mass) and τ is the collisional timescale. In the limit $\omega_c\,\tau \gg 1$, ions complete several orbits around magnetic field lines between collisions, and therefore $\nu_0 \gg \nu_{3,4} \gg \nu_{1,2}$. For typical plasma parameters of Tycho's shock front, and $H \simeq 10^{-4}$Gauss,

$$\omega_c\,\tau \sim 10^{10} \gg 1 \tag{17}$$

thus making all other tensor coefficients absolutely negligible when compared with ν_0.

For the case of a uniform magnetic **H** at an angle β with the normal to the interface, the role played by ν in Eq. (2), should be replaced by $\nu \to 3\,\nu\,sin^2\beta\,cos^2\beta$. As a result, the viscous effect is typically of the same order of magnitude than in the non-magnetic case. Notwithstanding, note that for the singular cases of magnetic field tangential to the interface ($\beta = 90°$) or magnetic field normal to the interface ($\beta = 0°$), the viscous effect is completely inhibited.

In summary, to properly include viscous effects in the R-T instability rate when strong magnetic fields are present (i.e. $\omega\tau \gg 1$), an extra term should be added in coefficient c_2 [see Eq. (13)], namely

$$c_{2\,\nu} = 6\,\nu\,sin^2\beta\,cos^2\beta\,k^2 \tag{18}$$

Fig. 5 shows the instability rate as a function of wavenumber, for various magnetic intensities. In particular, the values of k_* and γ_* (which correspond to the maxima of these curves) remain virtually unaffected by the magnetic intensity.

4. Results

In this section we assign particular values to the various parameters in Eqs. (10) and (11), to estimate the wavelength and growth time for the fastest growing perturbation.

We determine densities and temperatures based on different X-ray observations of Tycho's remnant. Spectral information

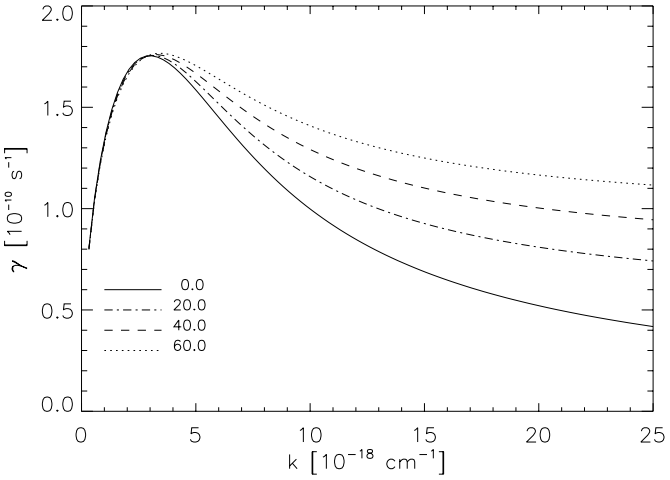

Fig. 5. R-T instability including oblique magnetic field and viscous effects, with $g_2 = 7.0$, $d_1 = 1.9$, $\alpha = 0.33$, $T_7 = 3.0$. Different traces correspond to different values of the magnetic field intensity in units of 10^{-6} gauss.

was used to derive temperatures, while density distribution was obtained from images.

High resolution images of Tycho's SNR from *Einstein* data were generated by Seward et al. 1983 . They identified three different origins for the X-ray radiation with distinct morphological characteristics, which they respectively associated with: a) shocked ISM b) diffuse ejecta and c) clumps. Considering that the X-ray luminosity, L_X, is produced by optically thin thermal bremsstrahlung,

$$L_X = n^2 P(T) V \tag{19}$$

where n is the particle density, V is the emitting volume and $P(T) \propto T^{-1/2}$ is the function of radiative losses for a plasma at temperature T. Seward et al. 1983 measured L_X and V for each of the sources in their images. The particle densities from Eq. (19) can be obtained, after assuming the temperatures for these emitting sources.

Later on, Tsunemi et al. 1986, Smith et al. 1988, Fink et al. 1994 and Vancura et al. 1995 performed high spectral resolution observations of this SNR. These studies allow them to fit the observed X-ray spectra with various theoretical spectra. Tsunemi et al. 1986 used data from the satellite *Tenma* for photon energies from 1 keV to 10 keV. They fit the observed X-ray spectrum assuming a thermal bremsstrahlung component and a non-equilibrium ionization model for the spectral lines. Their best fit corresponds to a temperature of $T \sim 2.9$ keV. Using *EXOSAT* data for a narrower range from 5 keV to 10 keV, Smith et al. 1988 obtained a temperature of $T \sim 6.5$ keV. Fink et al. 1994 find that the spectrum observed by *Ginga* from 2 keV to 20 keV, cannot be fitted by a single thermal source. Instead it can reasonably be adjusted by two thermal sources: a hot component ($T \sim 11$ keV) generally associated to the principal shock, and a relatively cooler component ($T \sim 2.7$ keV) which corresponds to both the diffuse ejecta and the dense clumps. The hot component dominates at energies above 10 keV, and it becomes gradually negligible as we go to lower energies. This effect might explain the differences between the temperatures predicted by Tsunemi et al. 1986 and Smith et al. 1988. The analysis of Vancura et al. 1995 from *BBXRT (Broad Band X-Ray Telescope)* data in the 1-9 keV range, yields a temperature estimate of 1.7 keV.

In the present work, we combine the results derived from the different observational studies to obtain reliable estimates for the temperature and density contrast at the contact discontinuity in the Tycho SNR. To this end, we assume as working hypothesis: *(i)* equal pressures at both sides of the discontinuity, *(ii)* the low density and high temperature plasma in the piston region is associated to the "diffuse ejecta" X-ray component, *(iii)* the higher density and lower temperature material right outside the contact discontinuity is related to the "clump" component. The associations made in our assumptions *(ii)* and *(iii)*, only mean that their X-ray emitting features are expected to be similar. Under these assumptions, we can derive approximate expressions for the density contrast:

$$\left(\frac{n_p}{n_s}\right)^{5/2} = \frac{\left(L_X/V\right)_p}{\left(L_X/V\right)_s} \tag{20}$$

since pressure balance implies

$$\frac{T_p}{T_s} \simeq \frac{n_s}{n_p} \tag{21}$$

The densities n_p and n_s have been derived from Eq. (19), using luminosities and volumes estimated by Seward et al. 1983 (re-scaled to 4.6 kpc) and temperatures from various spectral studies (see Table 1).

For the effective gravitational field intensity, we assume g_2=7, following the numerical calculations from Gull 1973, Gull 1975 and Dickel et al. 1989 .

After replacing the temperatures derived by various authors from spectral X-ray analysis into Eq. (10) and (11), we calculated the wavelength and growth time of the fastest growing mode. Our results are summarized in Table 1, where also the values derived from the radio observations (see below) are included. The computed densities (n_p and n_s) go as $d_{4.6}^{-1/2}$, while the theoretical wavelength λ_*, and the characteristic time, τ_*, depend on the distance as $d_{4.6}^{1/3}$ and $d_{4.6}^{1/6}$, respectively. The adimensional parameter $d_{4.6}$ indicates that $d_{4.6} = d/4.6kpc$.

By simply measuring the period of the wavy structure toward the northeast side of the shock front (see Fig. 2), and assuming a distance for Tycho's SNR of 4.6 kpc (Schwarz et al. 1995), we can derive a wavelength of:

$$\lambda_{obs} = (40 \pm 3)'' = (0.89 \pm 0.08) \times d_{4.6}\mathrm{pc} \tag{22}$$

where the quoted error corresponds to two VLA beams. The growth time can be compared with the time elapsed since Tycho's remnant entered the Sedov phase, which can be estimated as $\Delta\tau = t_{explosion} - t_c \approx 120$ years with

$$t_c = \left(\frac{1}{2\,E_*}\right)^{1/2} \left(\frac{3\,M_*^{5/2}}{4\,\pi\,n_{is}}\right)^{1/3} = 208\,\frac{(M_*/M_\odot)^{5/6}}{E_{51}^{1/2}\,n_{is}^{1/3}}\,\mathrm{yrs}. \tag{23}$$

Table 1.

n_p (cm^{-3})	n_s (cm^{-3})	T_7(K)	λ_*(pc)	τ_*(yrs)	References
3.1	1.5	3.4±0.3	1.00±0.20	200±20	a
3.2	1.5	3.8±0.3	1.20±0.30	210±20	b
3.1	1.5	$3.1^{+1.3}_{-1.8}$	$0.91^{+0.60}_{-0.80}$	190^{+70}_{-110}	c
2.7	1.3	2.0	0.50	140	d
			0.89±0.08	120	e

References: a) Tsunemi et al. 1986 ; **b)** Smith et al. 1988 ; **c)** Fink et al. 1994 ; **d)** Vancura et al. 1995 and **e)** Present VLA observations

where $M_* = 1.9\ M_\odot$, $E_{51} = E_*/(10^{51}\ \mathrm{ergs}) = 1.4$ and $n_{is} = 0.5\ \mathrm{cm}^{-3}$ from Seward et al.'s (1983) results scaled to a distance of 4.6 kpc. The time t_c corresponds to the situation where the mass of interstellar material swept by the piston becomes comparable to the mass M_* of the progenitor. At this stage, the deceleration of the piston is non-negligible and therefore the R-T modes enter into the unstable regime.

5. Conclusions

We have shown that the development of the Rayleigh-Taylor instability is feasible at the contact discontinuity of Tycho's SNR, which is consistent with similar results obtained by Chevalier et al. 1992 for a spherical geometry. By assuming typical values of the physical parameters involved, we obtain that the observed wavelength of 0.9 pc is fully, compatible with the theoretical prediction of a R-T instability with the inclusion of viscous effects, still in the linear stage of its evolution. As indicated in Eq. (22), the observed wavelength is proportional to Tycho's distance. On the other hand, the theoretically derived wavelength (Eq. (10)) also depends on the distance. Therefore, the coincidence between the observed and theoretical wavelengths, relies on good determination for Tycho's distance.

The addition of magnetic effects do not affect the non-magnetic study in any significant fashion. Also, we derive an instability growth time of 100-200 years (see Table 1), which indicates that the R-T instability is still in its linear stage.

The role of nonlinearities at this stage of Tycho's evolution might indeed be non-negligible, and therefore a numerical code including both nonlinear and viscous effects would provide a more accurate description. However, since the observed wavelength and growth time are consistent (within uncertainties) with the predictions presented here, if nonlinear effects exist, they do not seem to play a dominant role at this stage.

Notwithstanding, it is expected that over the next few hundreds of years the instability will enter to its nonlinear stage and the small protrusions observed will develop into longer filaments, similar to those observed in the Crab Nebula, but pointing in the opposite direction (i.e. outwards).

Deep optical images may reveal faint optical counterparts of the radio signatures of the R-T instability taking place in Tycho's SNR. As a final remark, we find that the radio study performed with good angular resolution and high sensitivity, is a promising tool to investigate fluid instabilities at different stages of their development.

Acknowledgements. We sincerely acknowledge an anonymous referee for very fruitful comments, which contributed to improve an earlier version of this manuscript. The observations shown in this paper were acquired as a part of a Cooperative Science Program between NSF (USA) and CONICET (Argentina). This work was partially funded by CONICET through the grant PMT-PICTO 107. D.G. acknowledges partial support from the University of Buenos Aires (grant EX247) and to Fundación Antorchas.

References

Blake, G.M. 1972, MNRAS, 156, 67.
Braginskii, S.S. 1966, 1, Reviews of Plasma Physics. (Consultants Bureau, New York).
Chandrasekhar, S. 1961, Hydrodynamic and Hydromagnetic Stability. (Oxford: Oxford Univ. Press).
Chevalier, R.A., Blondin, J.M., and Emmering, R.T. 1992, ApJ, 392, 118.
Cowie, L.L. 1975,MNRAS, 173, 429.
Dickel, J.R, Eilek, J. A, Jones, E. M. and Reynolds, S. P. 1989, ApJ, 370, 497.
Dickel, J.R., van Breugel, W.J.M. and Strom, R.G. 1991,AJ, 101(6), 2151.
Fink, H.H., Asaoka, I., Brinkmann, W., Kawai, N. and Koyama, K. 1994, A&A, 283, 635.
Friedman, E.A. 1954, ApJ, 120, 18.
Fryxell, B., Müller, E., and Arnett, D. 1991, ApJ, 367, 619.
Gardner, C.L., Glimm, J., McBryan, O., Menikoff, R., Sharp, D.H. and Zhang, Q. 1988, Phys.Fluids, 31, 447.
Glimm, J. Li, X.L. and Zhang, Q. 1990, Phys.Fluids A, 2, 2046.
Gull, S.F. 1973, MNRAS, 161, 47.
Gull, S.F. 1975, MNRAS, 171, 263.
Hester, J. J, et al., 1996, ApJ, 456, 225.
Hwang, U. and Gotthelf, E. V. 1997, ApJ, 475, 665.
Jones, E.M., Smith, B.W. and Straker, W.C., 1981, ApJ, 249, 185.
Jun, B.I.,Norman, M.L. and Stone J. M. 1995, ApJ, 453, 332.
Landau, L.D. and Lifshitz, E.M. 1959, "Fluid Mechanics", Pergamon Press, London
Li, X.L. 1993, Phys.Fluids A, 5, 1904
Matsui, Y., Long, K., Dickel, J. and Greisen, E. 1984, ApJ, 287, 295.
Milne, D.K. 1987, AuJph, 40, 771.
Newman, W.I. 1980, ApJ, 236, 880.
Plesset, M.S. and Whipple, C.G. 1974, Phys.Fluids, 17, 1.
Raymond,J.C. 1984, ARA&A, 22,75.
Read, K.I. 1984, Physica D, 12, 45.
Reynoso, E.M., Moffet, D.A., Goss, W.M., Dubner, G.M., Giacani, E.B., Reynolds, S.P. and Dickel, J.R. 1997, ApJ, 491, 816.
Reynoso, E.M., Velázquez, P.F., Dubner, G. M. and Goss, W.M. 1998, in preparation.
Schwarz, U.J., Goss, W.M., Kalberla, P.M. and Benaglia, P. 1995, A&A, 299, 193
Sedov, L.I. 1959, Similarity and dimensional methods in mechanics, Academic Press, New York.
Seward, F., Gorenstein, P. and Tucker, W. 1983,ApJ, 266, 287
Sharp, D.H. 1984, Physica D, 12, 3.
Smith, A., Davelaar, J., Peacock, A., Taylor, B.G., Morini, M. and Robba, N.R. 1988, ApJ, 325, 288.
Spitzer, L. 1962, Physics of Fully Ionized Gases, Willey, New York.

Stone, J.M. and Norman, M.L. 1992, ApJ, 390, L17.
Taylor, G.I. 1950, Proc. R. Soc. London, A201, 159
Tsunemi, H., Yamashita, K., Masai, K., Hayakawa, S. and Koyama, K. 1986, ApJ, 306, 248.
Vancura, O., Gorenstein, P. and Hughes, J.P. 1995, ApJ, 441, 680.
Woltjer, L. 1970, I.A.U. Symp. 39, 229, Reidel:Dordrecht
Youngs, D.L. 1984, Physica D, 12, 32.
Youngs, D.L.1989, Physica D, 37, 270.
Youngs, D.L.1991, Phys.Fluids A, 3, 1312.